Chapter 10
Silver Nanoparticles in Natural Environment: Formation, Fate, and Toxicity

Virender K. Sharma and Radek Zboril

Abstract In recent years, there has been growing interest in the existence of natural nanoparticles in the environment and their subsequent influence to the ecological health. This chapter presents the current status on thermally- and light-induced formation of silver nanoparticles (AgNPs) under environmentally relevant conditions. Influenced environmental parameters include temperature, pH, oxic/anoxic environment, and concentrations of precursors Ag^+ ions and natural organic matter (NOM). Surface-catalyzed reduction of Ag^+ could describe the formation of AgNPs under various conditions. The redox species of iron (Fe(II)/Fe(III)) in the thermally induced processes enhanced the formation of AgNPs. Moieties of NOM, Ag–NOM complexes, and reactive oxygen species, ROS (e.g., $O_2^{\cdot -}$) were provoked to explain the formation of AgNPs. Stability studies on formed AgNPs from Ag(I)–NOM reaction mixtures have shown their stability for days to several months. However, cations of the natural waters such as Na^+, K^+, Mg^{2+}, and Ca^{2+} can destabilize the AgNPs. A preliminary investigation on the toxicity of AgNPs, formed in the mixture of Ag^+-humic acid, suggests that lower minimum inhibition concentration against Gram-negative bacteria and Gram-positive bacteria compared to engineered AgNPs.

Keywords Noble metals · Natural nanoparticles · Organic matter · Stability · Toxicity

V.K. Sharma (✉)
Program for the Environment and Sustainability, Department of Environmental and Occupational Health, School of Public Health, Texas A&M University, College Station, TX 77843, USA
e-mail: vsharma@sph.tamhsc.edu

V.K. Sharma · R. Zboril
Regional Centre of Advanced Technologies and Materials, Departments of Experimental Physics and Physical Chemistry, Faculty of Science, Palacký University in Olomouc, 771 46 Olomouc, Czech Republic

B. Yan et al. (eds.), *Bioactivity of Engineered Nanoparticles*,
Nanomedicine and Nanotoxicology, DOI 10.1007/978-981-10-5864-6_10

10.1 Introduction

Engineered nanoparticles (ENPs) are widely used in development of technologies and in consumer products such as agriculture, electronic devices, and renewable energies [1–7]. ENPs synthesized in worldwide laboratories can be given as metals, metal oxides, metal sulfides, nonmetals, lipids, and polymers [8–10]. ENPs have been suggested to remediate polluted water [11, 12]. Iron-based nanoparticles are proposed in cancer treatment [13–15]. Because of many human health related applications of nanoparticles, synthesis of ENPs through reduction of metal salts with green chemistry reducing agents have been emphasized in order to protect the environment [5, 16–19]. Significantly, a role of environmental-friendly compounds to act as a stabilizing agent has also been investigated in detail [4, 10, 20]. Sugars and vitamins can act as both capping agents and thus represent examples of such compounds.

Among the category of metals, silver nanoparticles (AgNPs) have shown the most use in industrial and medical fields [1, 7, 21]. AgNPs have been found in more than 400 consumer products [22, 23]. After the intended use of AgNPs, the nanoparticles release into the environment [24–28]. Numerous investigations have been conducted on the fate and behavior of release of AgNPs into the aquatic environment, because of their effects on ecosystems and humans [8, 22, 26, 29, 30]. Comparatively, little is known on the mechanism of natural occurrence of AgNPs in different environmental conditions [31, 32]. Reactions in hydrothermal vents, surface water, and wastewater, and mining activities are possible processes that lead to natural formation of AgNPs in the environment [8, 33]. Significantly, the naturally formed AgNPs may also equally affect the ecological health of the environment [10, 34]. This chapter summarizes the results obtained on the formation of AgNPs under environmental conditions, followed by their fate and potential toxicity to the biological species.

10.2 Thermally Induced Formation of AgNPs

In this set of experiments, initial measurements on thermally induced formation of AgNPs were conducted at varied environmental conditions (Fig. 10.1) [35]. Solutions of Ag^+ were mixed with Suwannee River humic acid (SRHA) at different temperatures under different concentrations of SRHA and silver ions. It was observed that the color of the mixed solution changed with time from a light yellow color of the HA solution to strong yellow color. Spectra of the mixed solution were measured by UV–vis spectroscopy (Fig. 10.1a–c). The intense yellow color was from the surface plasmon resonance (SPR) of the AgNPs. The intensity of the SPR was dependent on the reaction conditions. When concentration of SRHA in mixed solution was increased by keeping concentration of Ag^+ at 90 °C, the intensity of SPR peak increased (Fig. 10.1a). An increase in temperature also enhanced the

growth of AgNPs (i.e., increase in the intensity of SPR) (Fig. 10.1b). When the level of Ag^+ in mixed solutions was increased by keeping the concentration of SRHA constant at 90 °C, the formation of AgNPs increased (Fig. 10.1c).

Figure 10.1a–c shows that the location of the peak wavelength and shape of the spectra depended on the initial concentration of SRHA and temperature. It seems that the location of the peak was a function of the diameter and agglomeration of the AgNPs. The peak was sharper with increased concentrations of SRHA at a constant Ag^+ concentration and temperature (Fig. 10.1a). This suggests that less polydisperse AgNP size distributions at high levels of SRHA. An increase in temperature of the mixed solution of Ag^+–SRHA enhanced growth of AgNPs and the peak became narrow (Fig. 10.1b). It was obvious that the formation mechanism of AgNPs was more likely operational at higher temperature. Low levels of Ag^+ also

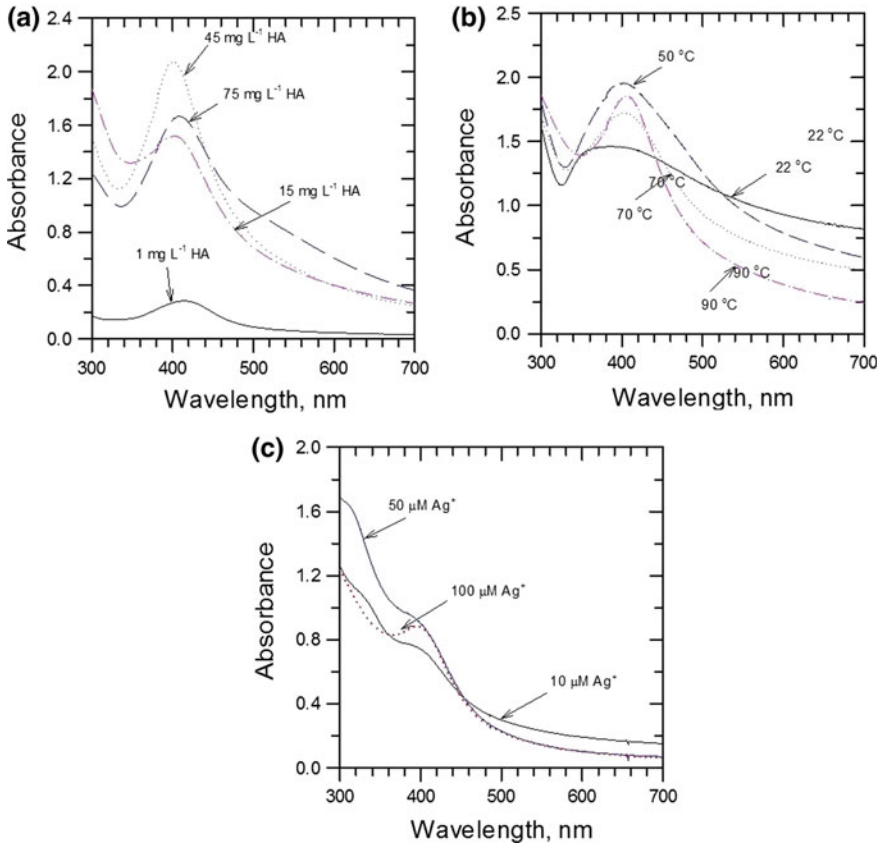

Fig. 10.1 UV-Vis absorption spectra of AgNPs. **a** Different [HA], $[Ag^+] = 1 \times 10^{-3}$ M, reaction time = 90–330 min, t = 90 °C; **b** different reaction temperatures, $[Ag^+] = 1 \times 10^{-3}$ M, [HA] = 100 mg L^{-1}; and **c** different $[Ag^+]$, t = 90 °C, [HA] = 100 mg L^{-1}. Adapted from [35] with the permission of American Chemical Society

showed the AgNPs (Fig. 10.1c). However, the peak of SPR was less defined (Fig. 10.1c).

In the next series of experiments, similar studies were conducted using Suwannee River fulvic acid (SRFA) [36]. Similar results, shown in Fig. 10.1, were observed. Increase in concentrations of Ag^+ and SRFA in mixed solutions and temperature resulted in the increase in intensity of SPR peak of the AgNPs. At high temperature of 90 °C, formation of AgNPs occurred in hours (or minutes) with well-defined SPR peak. Comparatively, it takes days to result in AgNPs at room temperature (25 °C). The SPR peaks were much broader at room temperature because of considerable polydispersity in size and local dielectric environment of the AgNPs [36]. Additional experiments were performed by varying the pH of the mixed solution [36]. Results demonstrated the increase in the formation of AgNPs with increase in pH (Fig. 10.2) [36]. With increase in pH, the shape of the SPR peaks of AgNPs was also broadened.

Results of Figs. 10.1 and 10.2 were understood by monitoring of the SPR peak of the AgNPs as a function of time intervals (Fig. 10.3) [36]. The shape of the curve seen in Fig. 10.3 suggests an autocatalytic process for the growth of AgNPs. Equation 10.1 was used to explain the process of the formation of AgNPs. Basically, Ag^+ ions from the bulk solution first adsorb onto a small cluster Ag_n before reduction by SRFA (or SRHA) to catalyze the growth of AgNPs.

$$Ag^+ + Ag_n + \text{SRFA(or SRHA)} \rightarrow Ag_{n+1} + \text{SRFA(ox)(or SRHA(ox))} \quad (10.1)$$

The autocatalytic process is described by Eq. 10.2.

$$\ln(a/(1-a)) = (k[Ag^+])t - \ln([Ag^+]/n[Ag_n]), \quad (10.2)$$

where $a = A_t/A_\infty$, and A_t and A_∞ are the absorbance values at time t and ∞, respectively. A linear relationship between ln $(a/(1-a))$ and the reaction time support that the formation of AgNPs results from an autocatalytic reaction in the Ag^+–SRHA or Ag^+–FA mixtures mixture solutions of Figs. 10.1 and 10.2.

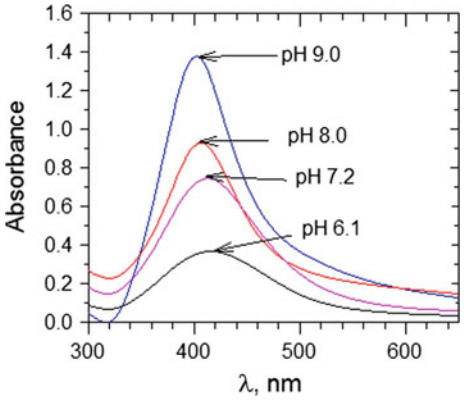

Fig. 10.2 UV-Vis absorption spectra of AgNPs in SRFA at different pH in 2 h heating at 90 °C. $[Ag^+]$ = 1×10^{-3} mol L^{-1}, 100 mg L^{-1} SRFA. Adapted from [36] with the permission of American Chemical Society

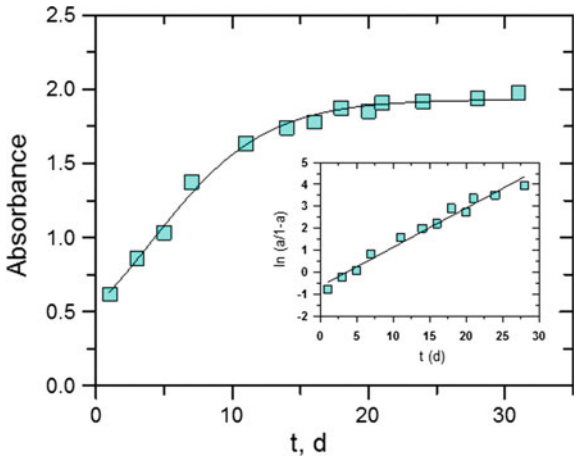

Fig. 10.3 Plot of absorbance versus time for the formation of AgNPs at 22 °C. $[Ag^+] = 1 \times 10^{-3}$ mol L^{-1}, 100 mg L^{-1} SRFA. *Inset* Plot of $\ln(\alpha/1 - \alpha)$ versus time. Adapted from [36] with the permission of American Chemical Society

The formation of AgNPs through the autocatalytic process was also confirmed by determining the thermodynamic feasibility of the reaction of Ag^+ ion and SRFA (or SRHA) under homogeneous solutions. The redox potentials for FA and HA are −0.5 and −0.7 V, respectively (Table 10.1) [37–43], which are not sufficient to overcome the highly negative redox potential of Ag^+ ions to isolated silver ($Ag^+ + e^- \rightarrow Ag^o$; $E^o = -1.8$ V vs. NHE) [38]. Therefore, direct reduction of Ag^+ ion by either SRFA or SRHA in solution mixture is not possible. However, it is likely that Ag^+ ions deposited on solid surfaces are being reduced by SRFA (or SRHA) due to a more positive redox potential. This idea stimulated from the known redox potential for reducing Ag^+ onto a Ag electrode is +0.8 V [37]. The steps of the mechanism of the formation of AgNPs may be written by Reactions (10.3–10.7).

$$2Ag^+ + 2OH^- \rightarrow Ag_2O + H_2O \quad \text{fast} \tag{10.3}$$

$$Ag_2O + (Ag^+)_n \rightarrow Ag_2O - (Ag^+)_n \quad \text{fast} \tag{10.4}$$

$$Ag_2O - (Ag^+)_n + FA \rightleftharpoons Ag_2O - (Ag^+)_n{-}FA \quad K_{ad} \tag{10.5}$$

$$Ag_2O - (Ag^+)_n{-}FA \rightarrow Ag_2O - (Ag^+)_{n-1} + Ag^o + FA^-(ox)k_{red} \tag{10.6}$$

$$Ag^o + Ag^o \rightarrow Ag_2 \quad \text{fast} \tag{10.7}$$

In this proposed mechanism, initial formation of colloidal Ag_2O occurred from the reaction between Ag^+ and OH^- ions (Reaction 10.3). The solid surface of Ag_2O thus adsorbed Ag^+ ion (Reaction 10.4), which could satisfy the thermodynamic feasibility condition of reduction of Ag^+ ion by SRFA (or SRHA) (Reactions 10.5 and 10.6). According to the mechanism, SRFA was adsorbed first onto colloidal particle of Ag_2O before reducing Ag^+ ion to metallic silver. The formation of

Table 10.1 Redox potentials of possible reactions in the Ag^+–NOM–Fe system

Reaction	E^0 versus NHE (V)	References
$Ag^+ + e^- \rightleftharpoons Ag^o$	−1.8	[37]
$Ag^+ + Ag^o_\infty + e^- \rightleftharpoons Ag^o_\infty$	0.8	[38]
$Fe^{3+} + e^- \rightleftharpoons Fe^{2+}$	0.77	[40]
$Q + 2H^+ + 2e^- \rightleftharpoons HQ$	−0.699	[38]
$FA_{(ox)} + e^- \rightleftharpoons FA_{(Red)}$	~0.5	[42]
$HA_{(ox)} + e^- \rightleftharpoons HA_{(Red)}$	~0.7	[43]
$Fe^{III}(HS) + e^- \rightleftharpoons Fe^{II}(HS)$	−0.20 to 0.30	[40]

FA fulvic acid, *HA* humic acid, *HS* humic substances

dimers (Reaction 10.7) was proposed prior to stabilization of larger clusters [44]. The autocatalytic reduction of Ag^+ may represent the driving force to reach metastable (or "magic-sized") Ag_n clusters that are thermodynamically far more favored than smaller entities. In the growth period, the metastable silver clusters agglomerate to generate the characteristic yellow color of AgNPs.

It is clear that reaction step (10.6) is the rate-determining step of the mechanism. The reduction capacity of organic matter (FA or HA) derives the formation of AgNPs. The amount of AgNPs (or growth of AgNPs) is directly related to the concentrations of both Ag^+ ions and SRHA (Fig. 10.1) [35]. An increase in the pH (or more concentration of OH^- ions) in solution would increase the amount of colloidal Ag_2O that enhanced the rate of formation of Ag_2O–$(Ag^+)_n$ particles. This process thus ultimately yielded increase in amount of AgNPs with increase in pH of the solution. Other possibility is that the functional groups of aromatic fractions of FA generally are deprotonated species at higher pH. The deprotonated species have relatively higher electron density than functional groups of protonated species. The initial binding and complexation of Ag^+ ions by FA species is expected to increase with increase in pH. This process may increase the rate of the formation of AgNPs with increase in pH (Fig. 10.2) [36].

Next, the formation of AgNPs was investigated using HA, obtained or isolated from different sources, which include aquatic, sedimentary, and soil. Details of procedures to obtain HA are given elsewhere [35]. Figure 10.4 shows the results of the formation of AgNPs under different HA at RT and 90 °C while keeping concentrations of Ag^+ and HA constant [35]. SUWHA was from Suwannee River HA from an aquatic source. SR, LD, and M2 represent HA are from sediments while MB, FITJ, S1, and WM belong to sources of HA from soil. As expected, a distinct yellow color of AgNPs was observed at RT was in days (Fig. 10.4a). At 90 °C, the formation of AgNPs was seen within 90 min (Fig. 10.4b). The intensity of the peak of the AgNPs varied with the source of the HA. The organic content and moieties of the organic matter present in HA determine the variation in growth of the AgNPs. Interestingly, soil HAs had sluggish or no formation of AgNPs. It appears that the predominant aliphatic-based SHA and aquatic HA were more easily able to reduce Ag^+ to yield AgNPs than did aromatic-dominated soil HA. The difference in growth

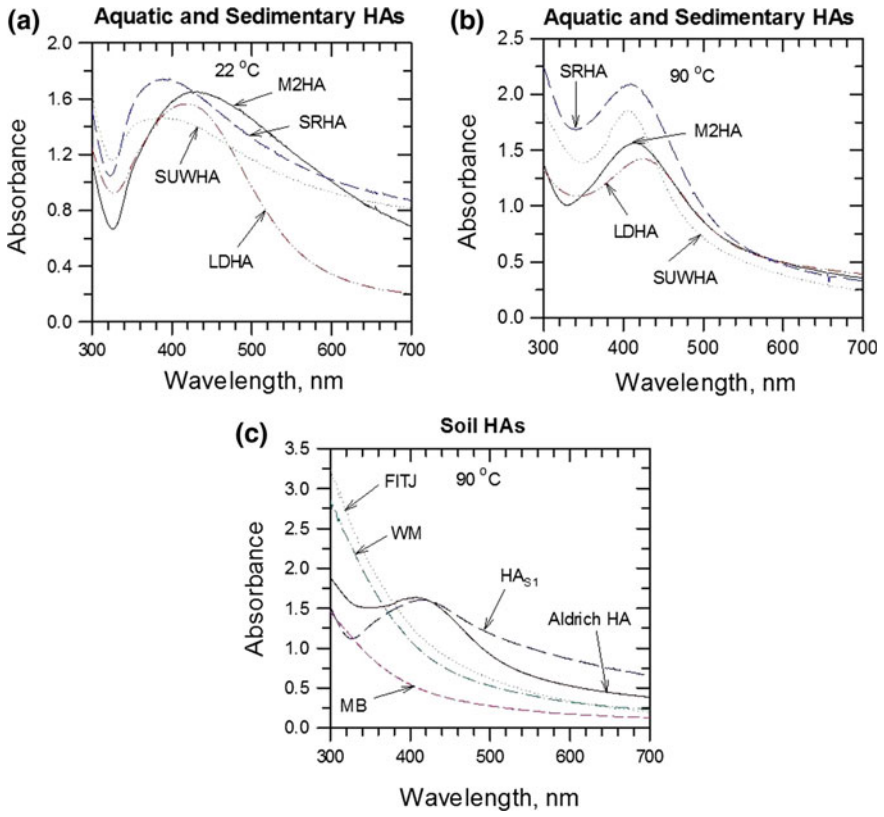

Fig. 10.4 UV-Vis absorption spectra of AgNPs. **a** Different aquatic/sedimentary HAs. $[Ag^+] = 1 \times 10^{-3}$ M, reaction time = 60–180 min, t = 22 °C, and [HA] = 100 mg L^{-1}; **b** different aquatic/sedimentary HAs. $[Ag^+] = 1 \times 10^{-3}$ M, reaction time = 60–180 min, t = 90 °C, and [HA] = 100 mg L^{-1}; and **c** different soil HAs, reaction time = 60–180 min, [HA] = 100 mg L^{-1}, $[Ag^+] = 1 \times 10^{-3}$ M, and t = 90 °C. Adapted from [35] with the permission of American Chemical Society

of AgNPs in sedimentary and soil samples may be described by the presence of the dominant form of reduced organic sulfides (thiols) in sedimentary HAs relative to the more oxidized form of organic sulfur present in soil HAs [45].

AgNPs obtained by the interaction of Ag^+ and HA were characterized by transmission electron microscopy, selected area electron diffraction (SAED), and atomic force microscopy (AFM) (Fig. 10.5) [35]. The shapes of the AgNPs were usually spherical with a very broad size distribution, ranging from diameters greater than 50 nm to less than 5 nm (Fig. 10.5a–d). The agglomeration of AgMPs was relatively more in the larger size AgNPs. The images of the AFM support the presence of crystalline AgNPs in the samples. Figure 10.3b demonstrates the [111] growth direction of the formed AgNPs. The high-resolution TEM (HRTEM) images in Fig. 10.5c indicates the presence of crystallites AgNPs. The SAED

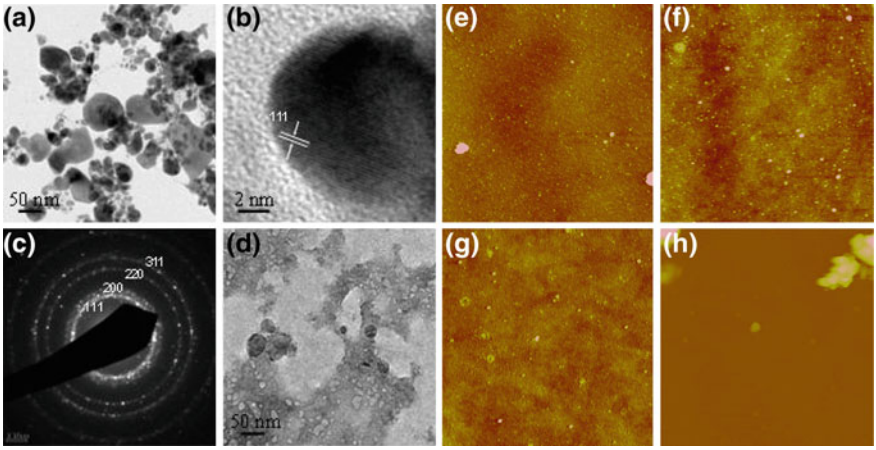

Fig. 10.5 Low resolution (**a**) and high resolution (**b**) TEM images of the AgNPs produced in the M2HA solution with the corresponding SAED pattern (**c**) of the Ag nanoparticles. Low-resolution TEM image of the as prepared M2HA solution is shown for comparison, and (**d**). The diffraction patterns can be precisely indexed to the face-centered cubic phase of Ag. AFM image of AgNPs formed by mixing $AgNO_3$ at room temperature with **e** M2HA, **f** SRHA, and **g**, **h** SUWHA for 6–13 days. *Scale bars* represent 400 nm, z-scale is 10 nm in (**e**–**g**) and 250 nm in (**h**). Adapted from [35] with the permission of the American Chemical Society

patterns and lattice planes seen can be indexed to face-centered cubic silver metal (Fig. 10.5c). Significantly, an abundance of amorphous natural colloids with equivalent electron density was observed (Fig. 10.5d). According to AFM images, AgNPs were singly dispersed spherical particles, mostly less than 10 nm in diameter (Fig. 10.5e–h). Significantly, images contained larger diameter particles that were less spherical (e.g., Fig 10.5f) or large agglomerates of many particles (e.g., Fig 10.5h).

The effect of iron species was explored by heating the mixture of Ag^+ with SRHA with and without Fe(II)/Fe(III) in solution at pH 6.0 and heated at 90 °C for 4 h [46]. The characteristic intense yellow color due to SRP of AgNPs appeared in mixed solutions (Fig. 10.6a). However, Fe^{2+} and Fe^{3+} species enhanced absorbance of SPR of AgNPs (Fig. 10.6a). Importantly, a mixed solution of only Ag^+ and Fe^{2+} without SRHA had no SPR of AgNPs (Fig. 10.6a). Significantly, there was no further enhancement in the SPR absorbance of AgNPs when the concentration of Fe^{2+} was increased (Fig. 10.6a). Similar results were observed at room temperature. However, the growth of AgNPs happened in several days, similar to results observed in Fig. 10.1.

The formation of AgNPs by the reduction of Ag^+ ion by either Fe^{2+} or SRHA is not thermodynamically possible due to the high negative potentials of the reactions (Eqs. 10.7 and 10.8) [37, 38, 40, 42, 43]. Surface auto-catalysis processes, described in Eqs. 10.3–10.7, were provoked to explain the formation of AgNPs.

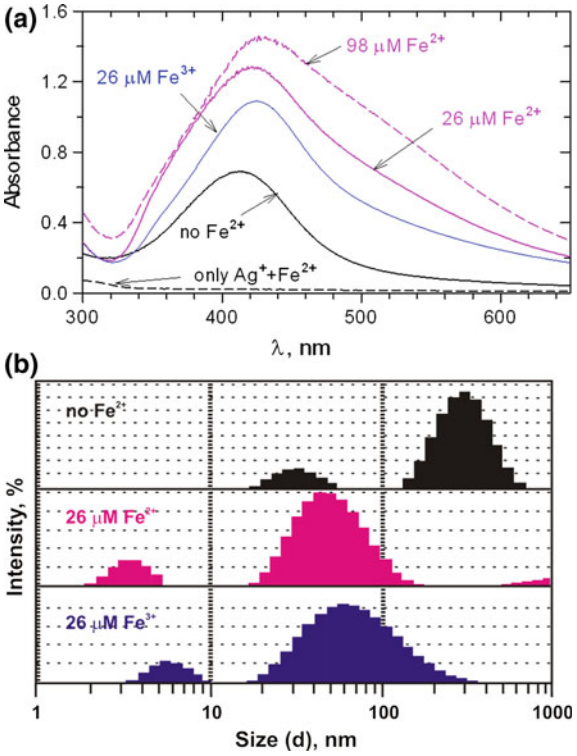

Fig. 10.6 UV-vis absorption spectra and DLS determined size distributions based on intensity fluctuation of AgNPs in Ag^+–SRHA solutions with and without Fe^{2+} and Fe^{3+} at pH 6.0. **a** UV-vis spectra and **b** DLS measurements. $[Ag^+] = 1 \times 10^{-3}$ mol L^{-1}, 40 mg L^{-1} SRHA. Adapted from [46] with the permission of American Chemical Society

$$Ag^+ + Fe^{2+} \rightleftharpoons Ag^o + Fe^{3+} \quad E^0 = -2.57\ \text{V} \tag{10.8}$$

$$Ag^+ + HA_{(Red)} \rightleftharpoons Ag^o + HA_{(Ox)} \quad E^0 = -2.50\ \text{V} \tag{10.9}$$

The presence of Fe^{2+} in the reaction mixture of Ag^+ and SRHA leading to a number of reactions can lead to number of reactions, which include the formation and dissociation of Fe(II)/Fe(III)-SRHA complexes and the formation of reactive oxygen species (ROS) $O_2^{\cdot-}$, H_2O_2, and $^{\cdot}OH$ [47–49]. These additional reactions helped to generate more amount of AgNPs in Ag^+–SRHA–Fe(II)/Fe(III) mixtures than in Ag^+–SRHA mixed solutions. For example, the complex formation of Fe^{2+} with NOM gave additional driving force to form AgNPs and thus enhanced the formation of AgNPs in the Ag^+–Fe^{2+}–SRHA mixed solution. This can be seen in positive redox potential of the Reaction (10.9). The reaction includes the redox potential of Fe(II)-HA/Fe(III)-HA system. The Reaction (10.9) provides additional step of the formation of AgNPs besides Reaction (10.7) without involvement of iron species to cause the increased formation of AgNPs (see Fig. 10.6a)

$$Ag^{+} + Ag^{o}_{\infty} + Fe^{II}(HS) \rightleftharpoons Ag^{o}_{\infty} + Fe^{III}(HS) \quad E^{0} \sim 0.5 - 1.0\ V \qquad (10.10)$$

The $O_2^{\cdot-}$ species, possibly formed in the reaction system, can also react with Ag^+ to yield an additional reaction to result in AgNPs.

Figure 10.6b shows the DLS measurements (intensity-based size distributions) of AgNPs in the absence and presence of iron in the Ag^+–SRHA system. The mean hydrodynamic diameter (HDD) of the AgNPs in the absence of iron was 201 nm. The HDD of AgNPs in the presence of consistent with faster growth of AgNPs in Ag^+–SRHA–Fe^{2+}/Fe^{3+} mixture solution than in Ag^+–SRHA. A polydisperse size distribution was seen in the polydispersity index (PI) of ~0.5 of the AgNPs (Fig. 10.6b).

The nature of natural organic matter (NOM) greatly influenced the growth of the formation of AgNPs in the Ag^+–NOM and Ag^+–NOM–Fe^{3+} systems (Fig. 10.7) [46]. In agreement with results of Fig. 10.6a, the presence of Fe^{3+} had higher amount of AgNPs formation than that in the absence of Fe^{3+} (Fig. 10.7). In the absence of Fe^{3+}, the relative ordering of the formation of AgNPs was NLFA > SRHA > SRFA (Fig. 10.7a). The composition of individual NOM, given in Table 10.2, was considered to understand the ordering of the growth of AgNPs. The carbon distribution and the content of functional groups did not provide clues of the ordering of growth rates of AgNPs (Fig. 10.7a and Table 10.2). Interestingly, the rate of the formation of AgNPs could be correlated with the free radical content order: NLFA, SRHA, and SRFA (see Table 10.2). It was suggested that the free radical species was involved in the initial formation of metallic silver (Reaction 10.6).

In the case of Ag^+–HA/FA–Fe^{3+} system, an increase in the growth of AgNPs for all HA and FAs was observed compared to Ag^+–HA/FA (Fig. 10.7a vs. 10.7b). However, the trend of the growth of AgNPs was SRHA > NLFA > SRFA, which

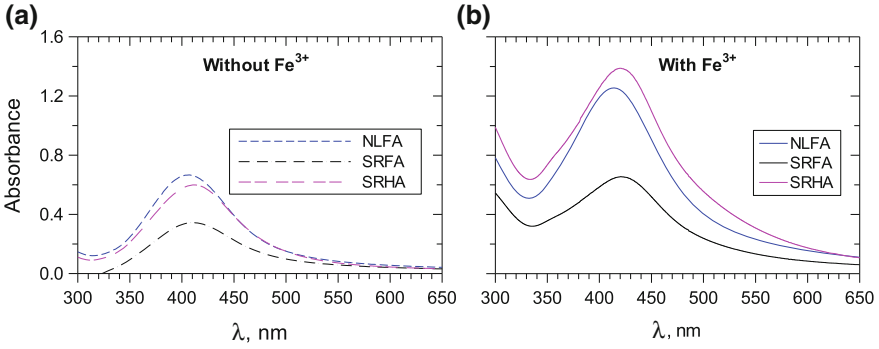

Fig. 10.7 UV-Vis absorption spectra of AgNPs in reduction of Ag^+ by different organic matter with and without Fe^{2+} at pH 6.0. A-without Fe^{2+} and B-with Fe^{3+} ($[Ag^+] = 1 \times 10^{-3}$ mol L^{-1}, [SRHA] = [SRFA] = [NLFA] = 40 mg L^{-1}, $[Fe^{3+}] = 13$ μM). Adapted from [46] with the permission of American Chemical Society

Table 10.2 Components present in different samples of FAs and HS

Sample	Function groups				^{13}C NMR estimates of carbon distribution content				Free radical
	Carboxyl	Phenolic	Carbonyl	Carboxyl	Aromatic	Acetal hetroaliphatic aliphatic			
	220–190 ppm	190–165 ppm	165–110 ppm	110–90 ppm	90–60 ppm	60–0 ppm			
SRHA	9.13	3.72	6	15	31	7	13	29	0.64[a]
SRFA	11.44	2.91	7	20	24	5	11	33	0.54
NLFA	11.16	3.18	10	24	31	7	12	18	1.14

SRHA Suwannee River II Humic Acid, *SRFA* Suwannee River I Fulvic Acid, *NLFA* Nordic Lake Fulvic Acid
[a]Reported for Suwannee River I Humic Acid

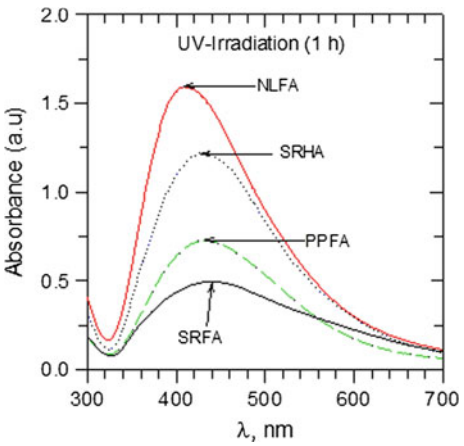

Fig. 10.8 UV-Vis absorption spectra of AgNPs for MRHW synthetic freshwater under UV irradiation for 1 h at pH 8.0. [Ag^+] = 1×10^{-3} mol L^{-1}, FA or HA = 45 mg L^{-1}). Adapted from [36] with the permission of the American Chemical Society

was different from the trend in the absence of Fe^{3+}. The Fe^{3+}-ligands complexation may have roles in the Ag^+–HA/FA–Fe^{3+} system. The complexation is usually driven by the nature and functional groups of the ligands [47]. Overall, reactions responsible to reduce Ag^+ to metallic silver are influenced by the nature of ligands to cause the trend seen in Fig. 10.7a.

10.3 Light-Induced Formation of AgNPs

Photochemical reactions involving metal species and natural organic matter represent a potential source for the natural formation of nanoscale particles in the environment [10, 50]. In our initial study, the UV light-induced formation of AgNPs was investigated (Fig. 10.8) [36]. The formation of the characteristic yellow color of AgNPs was clearly seen. The literature reports the photochemical formation of AgNPs under photosensitizers containing solution [51, 52]. Both fulvic and humic acids in the reaction mixtures may behave like photosensitizers to result in

the formation of AgNPs. Other possibility is that the formed Ag_2O in the reaction mixture (see Reaction 10.3) may act like a semiconductor [53]. The mechanism may involve the reduction of Ag^+ adsorbed onto Ag_2O by the photochemically generated reactive species such as hydrated electrons and $O_2^{-\cdot}$ in solution to yield AgNPs [48, 54]. The $O_2^{-\cdot}$ species can react with Ag^+ ions to form AgNPs [55]. It seems that the interactions among Ag^+, AgNPs and reactive species are causing the formation of AgNPs.

Significantly, the nature of organic matter was found to be important. For example, the use of different fulvic acids and humic acid showed the following order for the rate of formation: NLFA > SRHA > PPFA > SRFA [36]. This order is similar to the one seen in thermally induced formation of AgNPs using different sources of organic matter [35]. A few other studies have also shown the formation of AgNPs under UV and visible light irradiation [56]. The presence of Cl^- may enhance the formation of AgNPs from solid AgCl(s) in the presence of visible light. This is important considering natural levels of Cl^- ions in water. An earlier work on the formation of AgNPs from Ag(I)-NOM mixtures under UV light suggested the role of superoxide [56]. However, later work on sunlight-driven formation of AgNPs from the mixture of Ag(I)-NOM ruled out the possibility of superoxide to reduce Ag(I) ions [57]. The Ag(I)-NOM binding may be responsible in the sunlight-driven photoreduction of Ag(I) ions to AgNP [57].

More recently, the role of oxygen was probed by irradiating the mixed solution of Ag^+–HA at pH 6.0 under oxic and anoxic conditions. The formation of AgNPs nanoparticles at different time intervals is demonstrated in Fig. 10.9 [58]. The characteristic yellow color from the SPR of AgNPs had a broader peak features

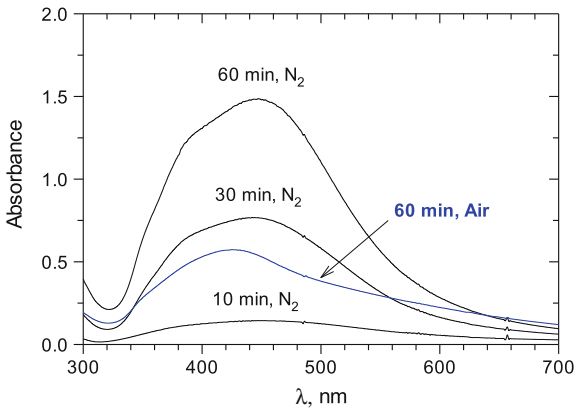

Fig. 10.9 Formation of silver nanoparticles from silver(I)-humic acid mixtures in 2-(*N*-morpholino)ethanesulfonic acid buffer at pH 6.0 under ultraviolet irradiation and nitrogen or air. This data shows that a process involving silver(I) ions binding to organic matter is suggested in the photoreduction of silver ion for silver particle in the environment. Experimental conditions: $[Ag^+] = 1.0 \times 10^{-3}$ mol L^{-1}, [HA] = 40 mg L^{-1}. Adapted from [58] with the permission of Springer Inc.

between 420 and 460 nm. The intensity of the peak increased gradually with time (Fig. 10.9). Significantly, the peak intensity under N_2 (i.e., anoxic condition) at 60 min was much more than the corresponding intensity under air (i.e., oxic conditions) at 60 min. This indicates dissolved oxygen may not be playing a dominant role in the formation of AgNPs under UV irradiation.

The effect of iron species (Fe(II)/Fe(III) on the UV-induced formation was studied by mixing 26 μM Fe(II) ion to a Ag^+–HA solution (Fig. 10.10) [46]. With Fe(II) solution in the anoxic solution, a sharp decrease in the AgNPs was observed (Fig. 10.10a). Other interesting feature was a much broader and more intense SPR of the AgNPs under anoxic conditions. This indicates that Fe(II) decreased the growth of AgNPs in the mixed solution, which caused the large particle size distribution and broad spectrum under anoxic conditions of Ag^+–HA–Fe(II) system. Furthermore, Fe(II) ions may be inhibiting the ligand-to-metal-charge transfer process to photoreduce silver ions to yield AgNPs (Fig. 10.10a). When a similar study was performed under oxic conditions, iron ions had almost no influence on giving AgNPs; in contrast to the thermally induced Fe(II) enhanced AgNPs formation [46]. This was not surprising because different mechanisms are generally involved in thermal- and photo-induced formation of AgNPs from the reduction of Ag^+ ion to metallic silver.

The influence of the valence state of iron (i.e., Fe(II) versus Fe(III) ion) on the formation of AgNPs was also explored by adding 26 μM Fe(II) and 26 μM Fe(III) ions into Ag^+–FA mixed solution, followed by UV irradiation. This study was carried out under anoxic conditions. The presence of Fe(II) caused broadening of the SPR peaked of the formed AgNPs. Also, no change in the intensity of SPR peak due to the presence of Fe(II) in the Ag^+–FA solution was seen (Fig. 10.10b). Comparatively, a decrease in the intensity of the AgNPs in the Ag^+–HA–Fe(II)

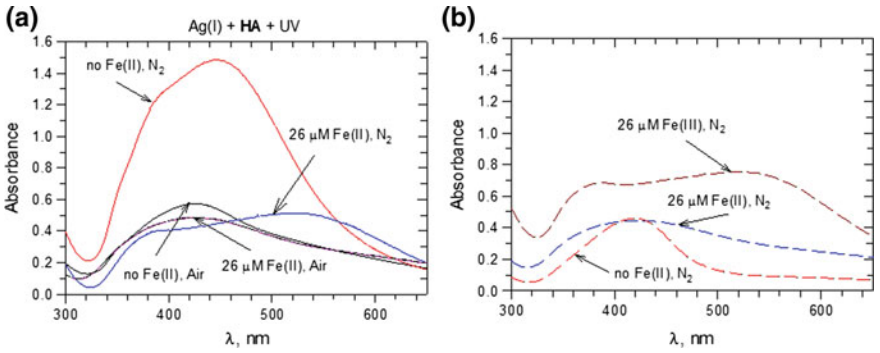

Fig. 10.10 Formation of silver nanoparticles during the ultraviolet irradiation of **a** silver(I)-humic acid-iron(II) purged with nitrogen and air at pH 6.0 and **b** silver(I)-fulvic acid-iron(II)/iron(III) purged with nitrogen at pH 6.0. The data shows that the influence of iron ions on the formation of silver particles from photoreduction of silver ions depends on the nature of the organic matter. Experimental conditions: $[Ag^+] = 1.0 \times 10^{-3}$ mol L^{-1}, [FA] = [HA] = 40 mg L^{-1}. Adapted from [58] with the permission of Springer Inc.

solution was observed (Fig. 10.10a). Humic and fulvic acids have different moieties, which would result in distinguished effects due to Fe(II) on the formation of AgNPs. In the case of Fe(III) ions in the mixture of Ag^+–FA solution, the formation of AgNPs had broader peak in comparison with no Fe(III) in the mixed solution of Ag^+ and FA. Further investigations are needed to comprehend the effect of iron species on the UV-induced formation of AgNPs in the mixture of Ag^+ and NOM.

10.4 Fate of AgNPs

In the beginning of our work on the syntheses of AgNPs, we focused on stabilization of the particles using surfactants, saccharides, and polymers [16]. These AgNPs were classified as engineered AgNPs. In recent years, we are interested in learning the fate of AgNPs formed from the interaction of Ag^+ with NOM under conditions of environmental relevance [35, 36, 46, 59]. Results of AgNPs formed from the reduction of Ag(I) by HA and FA with and without iron species in solution are presented in Fig. 10.11. Figure 10.11a shows the stability of AgNPs formed from the thermally induced reduction of Ag^+ by sedimentary and river HA. River HA had a decrease in stability of AgNPs up to 25% in 7 days. However, sediments HA showed only 7% in the same time period of 70 days. A blueshift in the SPR peak from 423 to 410 nm was noticeable (Fig. 10.11a). A similar stability trend of AgNPs resulted from the interaction of Ag^+ with FA was observed (Fig. 10.11b). Repulsive forces between negatively charged AgNPs (zeo potential varied only from −40 to −33 mV during seven months) was largely responsible for preventing the aggregation of particles and thus AgNPs were stable even for 7 months (Fig. 10.11b). More importantly, Fe^{3+} ions in the reaction mixtures of Ag^+–FA did not alter the stability of AgNPs (Fig. 10.11c). Interestingly, increase in SPR of AgNPs was noticed during 7-month period. In the presence and absence of Fe^{3+} ions, the values of zeta potential were −18 and −23 mV, respectively, in Ag^+–FA reaction mixture. This indicates that Fe^{3+} ion did not cause any significant change in the organic matter coated surfaces of AgNPs. It is likely that the coating of organic matter on AgNPs inhibits the dissolution of the nanoparticles, which ultimately result in increased stability of the AgNPs.

The presence of ions in solutions decreased the stability of AgNPs [29, 60]. The decreases in the stability of AgNPs were less in chloride salts of monovalent ions (Na^+ and K^+) than those of divalent cations (e.g., Mg^{2+} and Ca^{2+}) in solutions of Ag^+-organic matter [59]. An increase in ionic strength of solution also destabilized the AgNPs. This could be seen in decrease in the value of zeta potential of AgNPs from ~ -32 mV at 1 mM to ~ -15 mV at 10 mM $CaCl_2$ solution. Furthermore, the hydrodynamic diameter (HDD) of AgNPs increased from nm to μm in this ionic strength range, which showed that the agglomeration of the AgNPs increased with ionic strength of the electrolyte solution. The major finding of these results was that the natural organic matter stabilized AgNPs may become less stable as they move from freshwater to estuarine water and finally to seawater.

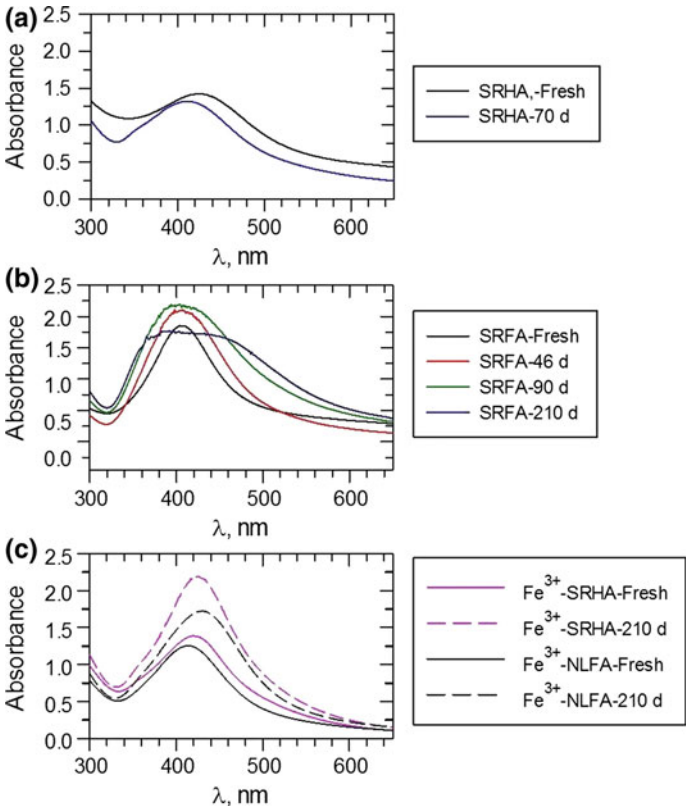

Fig. 10.11 UV-Vis measurements of aging of AgNPs formed at 90 °C. Days represent time after the formation of particles. **a** 100 mg L^{-1} SRHA, pH 8.0, **b** 100 mg L^{-1} SRFA; pH 8.0, and **c** Fe^{3+}–FA reaction mixtures, [SRHA] = [NLFA] = 40 mg L^{-1} SRFA. [Fe^{3+}] = 13 µM; pH 6.0) ([Ag^{+}] = 1 × 10^{-3} mol L^{-1}). Adapted from [36, 46, 59] with the permission of American Chemical Society

10.5 Toxicity

An investigation in our laboratory on the toxicity of thermally induced formation of AgNPs from the reduction of Ag^{+} by HA was conducted [46]. The minimum inhibitory concentrations (MIC) of HA-coated AgNPs against Gram-positive (GP) and Gram-negative (GN) bacteria were determined [46]. Selection of two kinds of bacteria was based on their distinct toxic effects against GP and GN bacterial species. Figure 10.12 shows the comparison of naturally formed AgNPs (i.e., HA-coated AgNPs) with ENPs (poly vinylpyrrolidone coated silver nanoparticles (AgNPs-PVP) and sodium dodecyl sulfate coated silver nanoparticles (AgNPs-SDS) [10, 16, 46]. Differences in toxicity of AgNPs against GN bacteria from GP bacteria species could be seen in Fig. 10.12. ENPs (AgNPs-PVP and

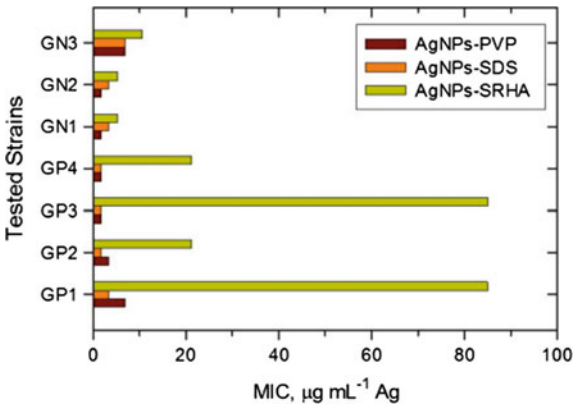

Fig. 10.12 Minimum inhibitory concentrations of engineered NPs (AgNPs-PVP and AgNPS-SDS) and natural AgNPs (AgNPs-SRHA) against Gram-positive (GP) and Gram-negative (GN) bacteria. *PVP* Poly vinylpyrrolidone; *SDS* Sodium dodecyl sulfate; *SRHA* Suwanee River humic acid; *GP1 Enterococcus faecalis* CCM 4224; *GP2 Staphylococcus aureus* CCM 3953; *GP3 Staphylococcus aureus* (MRSA); *GP4 Staphylococcus epidermidis* 1; *GN1 Pseudomonas aeruginosa* CCM; *GN2 Pseudomonas aeruginosa*; *GN3 Klebsiella pneumoniae* (ESBL). Adapted from [10] with the permission of the Royal Chemical Society

AgNPs-SDS) were more toxic than HA-coated AgNPs) (i.e., values of MIC were less in engineered AgNPs than MIC values obtained in naturally formed AgNPs). This difference in toxicity between ENPs and natural AgNPs was less pronounced for GN than GP species (Fig. 10.12). The organic coating produced on the AgNPs under conditions of natural environment may result in decreasing toxicity.

10.6 Conclusions

Several researchers have performed studies on the fate and behavior of the released engineered AgNPs into the environment in order to learn their health effects to humans and ecology. Comparatively, the formation and fate of naturally occurring AgNPs is rather sparse. AgNPs are formed by reduction of Ag^+ by NOM under thermal and photochemical conditions, followed by capping to ensure the stability of formed AgNPs. The surface-capped by NOM would be affected by pH, ions, and light. The interaction of naturally formed AgNPs, which are covered with bulky components of natural organic matter (NOM), with cell surface to cause toxicity is very likely different from the engineered AgNPs. The toxic mechanism may include the generation of ROS by AgNPs and direct and indirect damage to DNA by AgNPs and/or released Ag^+ ions. Genomic and proteomic approaches may be applied to comprehend ecotoxicological impacts of naturally formed AgNPs. Overall, more studies are needed to fully understand the formation and fate of

AgNPs under various environmental conditions (e.g., oxicic and anoxic) as well as their true toxic potential to ecological systems.

Acknowledgements V.K. Sharma and R. Zboril acknowledge the support by the Operational Program Research and Development for Innovations-European Regional Development Fund (CZ.1.05/2.1.00/03.0058). V.K. Sharma thanks the Program for the Environment and Sustainability.

References

1. Soenen SJ, Parak WJ, Rejman J, Manshian B (2015) (Intra)cellular stability of inorganic nanoparticles: effects on cytotoxicity, particle functionality, and biomedical applications. Chem Rev 115:2109–2135
2. Mu Q, Jiang G, Chen L, Zhou H, Fourches D, Tropsha A, Yan B (2014) Chemical basis of interactions between engineered nanoparticles and biological systems. Chem Rev 114:7740–7781
3. Bandyopadhyay S, Peralta-Videa JR, Gardea-Torresdey JL (2013) Advanced analytical techniques for the measurement of nanomaterials in food and agricultural samples: a review. Environ Eng Sci 30:118–125
4. Mohammadinejad R, Karimi S, Iravani S, Varma RS (2015) Plant-derived nanostructures: types and applications. Green Chem 18:20–52
5. Varma RS (2012) Greener approach to nanomaterials and their sustainable applications. Curr Opin Chem Eng 1:123–128
6. Rizzello L, Pompa PP (2014) Nanosilver-based antibacterial drugs and devices: mechanisms, methodological drawbacks, and guidelines. Chem Soc Rev 43:1501–1518
7. Stark WJ, Stoesset PR, Wohlleben W, Hafner A (2015) Industrial applications of nanoparticles. Chem Soc Rev 44:5793–5806
8. Philippe A, Schaumann GE (2014) Interactions of dissolved organic matter with natural and engineered inorganic colloids: a review. Environ Sci Technol 48:8946–8962
9. Quigg A, Chin WC, Chen CS, Zhang S, Jiang Y, Miao AJ, Schwehr KA, Xu C, Santschi PH (2013) Direct and indirect toxic effects of engineered nanoparticles on algae: role of natural organic matter. ACS Sustain Chem Eng 1:686–702
10. Sharma VK, Filip J, Zboril R, Varma RS (2015) Natural inorganic nanoparticles: formation, fate, and toxicity in the environment. Chem Soc Rev 44:8410–8423
11. Noubactep C, Caré S, Crane R (2012) Nanoscale metallic iron for environmental remediation: prospects and limitations. Water Air Soil Pollut 223:1363–1382
12. Sánchez A, Recillas S, Font X, Casals E, González E, Puntes V (2011) Ecotoxicity of, and remediation with, engineered inorganic nanoparticles in the environment. Trends Anal Chem 30:507–516
13. Zhang Y, Bai Y, Jia J, Gao N, Li Y, Zhang R, Jiang G, Yan B (2014) Perturbation of physiological systems by nanoparticles. Chem Soc Rev 43:3762–3809
14. Pati SS, Singh LH, Guimarães EM, Mantilla J, Coaquira JAH, Oliveira AC, Sharma VK, Garg VK (2016) Magnetic chitosan-functionalized Fe_3O_4@Au nanoparticles: synthesis and characterization. J Alloys Compd 684:68–74
15. Lohse SE, Murphy CJ (2012) Applications of colloidal inorganic nanoparticles: from medicine to energy. J Am Chem Soc 134:15607–15620
16. Panáček A, Kvítek L, Prucek R, Kolář M, Večeřová R, Pizúrová N, Sharma VK, Nevěčná T, Zbořil R (2006) Silver colloid nanoparticles: synthesis, characterization, and their antibacterial activity. J Phys Chem B 110:16248–16253

17. Sharma VK, Yngard RA, Lin Y (2009) Silver nanoparticles: green synthesis and their antimicrobial activities. Adv Colloid Interface Sci 145:83–96
18. Batley GE, Kirby JK, McLaughlin MJ (2013) Fate and risks of nanomaterials in aquatic and terrestrial environments. Acc Chem Res 46:I854–I862
19. Nadagouda MN, Iyanna N, Lalley J, Han C, Dionysiou DD, Varma RS (2014) Synthesis of silver and gold nanoparticles using antioxidants from blackberry, blueberry, pomegranate, and turmeric extracts. ACS Sustain Chem Eng 2:1717–1723
20. Virkutyte J, Varma RS (2011) Green synthesis of metal nanoparticles: biodegradable polymers and enzymes in stabilization and surface functionalization. Chem Sci 2:837–846
21. Alexander JW (2009) History of the medical use of silver. Surg Infect 10:289–292
22. Tang S, Wang M, Germ KE, Du HM, Sun WJ, Gao WM, Mayer GD (2015) Health implications of engineered nanoparticles in infants and children. World J Pediatr 11:197–206
23. Guo H, Zhang Z, Xing B, Mukherjee A, Musante C, White JC, He L (2015) Analysis of silver nanoparticles in antimicrobial products using surface-enhanced raman spectroscopy (SERS). Environ Sci Technol 49:4317–4324
24. Mitrano DM, Motellier S, Clavaguera S, Nowack B (2015) Review of nanomaterial aging and transformations through the life cycle of nano-enhanced products. Environ Int 77:132–147
25. Wigger H, Hackmann S, Zimmermann T, Köser J, Thöming J, von Gleich A (2015) Influences of use activities and waste management on environmental releases of engineered nanomaterials. Sci Total Environ 535:160–171
26. Lowry GV, Espinasse BP, Badireddy AR, Richardson CJ, Reinsch BC, Bryant LD, Bone AJ, Deonarine A, Chae S, Therezien M, Colman BP, Hsu-Kim H, Bernhardt ES, Matson CW, Wiesner MR (2012) Long-term transformation and fate of manufactured Ag nanoparticles in a simulated large scale freshwater emergent wetland. Environ Sci Technol 46:7027–7036
27. Krzyzewska I, Kyziol-Komosinska J, Rosik-Dulewska C, Czupiol J, Antoszczyszyn-Szpicka P (2016) Inorganic nanomaterials in the aquatic environment: behavior, toxicity, and interaction with environmental elements. Arch Environ Prot 42:87–101
28. Holden PA, Nisbet RM, Lenihan HS, Miller RJ, Cherr GN, Schimel JP, Gardea-Torresdey J (2013) Ecological nanotoxicology: Integrating nanomaterial hazard considerations across the subcellular, population, community, and ecosystems levels. Acc Chem Res 46:813–822
29. Sharma VK, Siskova K, Zboril R, Gardea-Torresdey J (2014) Organic-coated silver nanoparticles in biological and environmental conditions: Fate, stability and toxicity. Adv Colloid Int Sci 204:15–34
30. Ellis LJA, Valsami-Jones E, Lead JR, Baalousha M (2016) Impact of surface coating and environmental conditions on the fate and transport of silver nanoparticles in the aquatic environment. Sci Total Environ 568:95–106
31. Arturo Gómez-Caballero J, Guadalupe Villaseñor-Cabral M, Santiago-Jacinto P, Ponce-Abad F (2010) Hypogene Ba-rich todorokite and associated nanometric native silver in the San Miguel Tenango mining area, Zacatlán, Puebla, Mexico. Can Mineral 48:1237–1253
32. Wen LS, Santschi PH, Gill GA, Paternostro CL, Lehman RD (1997) Colloidal and particulate silver in river and estuarine waters of Texas. Environ Sci Technol 31:723–731
33. Gartman A, Findlay AJ, Luther GW (2014) Nanoparticulate pyrite and other nanoparticles are a widespread component of hydrothermal vent black smoker emissions. Chem Geol 366:32–41
34. Furtado LM, Bundschuh M, Metcalfe CD (2016) Monitoring the fate and transformation of silver nanoparticles in natural waters. Bull Environ Contam Toxicol 97:1–7
35. Akaighe N, MacCuspie RI, Navarro DA, Aga DS, Banerjee S, Sohn M, Sharma VK (2011) Humic acid-induced silver nanoparticle formation under environmentally relevant conditions. Environ Sci Technol 45:3895–3901
36. Adegboyega NF, Sharma VK, Siskova K, Zbořil R, Sohn M, Banerjee S (2013) Interactions of aqueous Ag^{+} with fulvic acids: mechanisms of silver nanoparticle formation and investigation of stability. Environ Sci Technol 47:757–764
37. Henglein A (1989) Non-metallic silver clusters in aqueous solution: stabilization and chemical reactions. Chem Phys Lett 154:473–476

38. Gentry ST, Fredericks SJ, Krchnavek R (2009) Controlled particle growth of silver sols through the use of hydroquinone as a selective reducing agent. Langmuir 25:2613–2621
39. Rose AL, Waite TD (2003) Kinetics of iron complexation by dissolved natural organic matter in coastal waters. Mar Chem 84:85–103
40. Rose AL, Waite TD (2003) Effect of dissolved natural organic matter on the kinetics of ferrous iron oxygenation in seawater. Environ Sci Technol 37:4877–4886
41. Rose AL, Waite TD (2003) Kinetics of hydrolysis and precipitation of ferric iron in seawater. Environ Sci Technol 37:3897–3903
42. Wilson SA, Weber JH (1977) A comparative study of number-average dissociation-corrected molecular weights of fulvic acids isolated from water and soil. Chem Geol 19:285–293
43. Struyk Z, Sposito G (2001) Redox properties of standard humic acids. Geoderma 102:329–346
44. Takesue M, Tomura T, Yamada M, Hata K, Kuwamoto S, Yonezawa T (2011) Size of elementary clusters and process period in silver nanoparticle formation. J Am Chem Soc 133:14164–14167
45. Kvítek L, Prucek R, Panáček A, Novotný R, Hrbáč J, Zbořil R (2005) The influence of complexing agent concentration on particle size in the process of SERS active silver colloid synthesis. J Mater Chem 15:1099–1105
46. Adegboyega NF, Sharma VK, Siskova KM, Vecerova R, Kolar M, Zboril R, Gardea-Torresdey JL (2014) Enhanced formation of silver nanoparticles in Ag^+–NOM–iron (II, III) systems and antibacterial activity studies. Environ Sci Technol 48:3228–3235
47. Jones AM, Pham AN, Collins RN, Waite TD (2009) Dissociation kinetics of Fe(III)- and Al (III)-natural organic matter complexes at pH 6.0 and 8.0 and 25 °C. Geochim Cosmochim Acta 73:2875–2887
48. Jones AM, Garg S, He D, Pham AN, Waite TD (2011) Superoxide-mediated formation and charging of silver nanoparticles. Environ Sci Technol 45:1428–1434
49. Rose AL, Waite TD (2002) Kinetic model for Fe(II) oxidation in seawater in the absence and presence of natural organic matter. Environ Sci Technol 36:433–444
50. Liu Z, Xie P, Ma J (2016) Aqueous photoproduction of Au nanoparticles by natural organic matter: effect of $NaBH_4$ reduction. Environ Sci Nano 3:707–714
51. Stamplecoskie KG, Scaiano JC (2012) Silver as an example of the applications of photochemistry to the synthesis and uses of nanomaterials. Photochem Photobiol 88:762–768
52. Sudeep PK, Kamat PV (2005) Photosensitized growth of silver nanoparticles under visible light irradiation: a mechanistic investigation. Chem Mater 17:5404–5410
53. Tselepis E, Fortin E (1986) Preparation and photovoltaic properties of anodically grown Ag_2O films. J Mater Sci 21:985–988
54. Wang W, Zafiriou OC, Chan IY, Zepp RG, Blough NV (2007) Production of hydrated electrons from photoionization of dissolved organic matter in natural waters. Environ Sci Technol 41:1601–1607
55. He D, Jones AM, Garg S, Pham AN, Waite TD (2011) Silver nanoparticle-reactive oxygen species interactions: application of a charging-discharging model. J Phys Chem C 115:5461–5468
56. Yin Y, Liu J, Jiang G (2012) Sunlight-induced reduction of ionic Ag and Au to metallic nanoparticles by dissolved organic matter. ACS Nano 6:7910–7919
57. Hou WC, Stuart B, Howes R, Zepp RG (2013) Sunlight-driven reduction of silver ions by natural organic matter: formation and transformation of silver nanoparticles. Environ Sci Technol 47:7713–7721
58. Adegboyega NF, Sharma VK, Cizmas L, Sayes CM (2016) UV light induces Ag nanoparticle formation: roles of natural organic matter, iron, and oxygen. Environ Chem Lett 14:353–357

59. Akaighe N, Depner SW, Banerjee S, Sharma VK, Sohn M (2012) The effects of monovalent and divalent cations on the stability of silver nanoparticles formed from direct reduction of silver ions by Suwannee River humic acid/natural organic matter. Sci Total Environ 441:277–289
60. El Badawy AM, Luxton TP, Silva RG, Scheckel KG, Suidan MT, Tolaymat TM (2010) Impact of environmental conditions (pH, ionic strength, and electrolyte type) on the surface charge and aggregation of silver nanoparticles suspensions. Environ Sci Technol 44:1260–1266